The Direct Wave-Drive Thruster

Matthew S. Feldman* and Edgar Y. Choueiri†

Electric Propulsion and Plasma Dynamics Laboratory, Princeton, New Jersey, 08544, USA

A propulsion concept relying on the direct acceleration of a plasma by momentum injection associated with the excitation of electrostatic waves is presented. The interaction between the wave-launching antenna and the plasma is investigated in order to evaluate the potential of this concept for propulsion. The total force from an annular antenna on a finite conductivity plasma slab is modeled analytically and determined to be a function of three non-dimensional parameters: the ratio of the electron collision frequency to the excitation frequency, the ratio of the antenna size to the antenna-plasma stand-off length, and the plasma skin-depth normalized by the size of the antenna. Calculations from the model show that total thrust improves for smaller electron collision frequencies, skin-depths, and stand-off distances. Thrust efficiency is also modeled and is dependent on the same non-dimensional parameters. The efficiency improves for smaller electron collision frequencies and stand-off lengths. The effect of the skin depth depends on whether the resistive losses in the exciting antenna are large or small, with smaller skin depths increasing efficiency when antenna losses are large. A sample evaluation is performed with the model to illustrate potential performance for a thruster operating at 5kW with a mass flow rate of 1 mg/s and found that for typical plasma parameters, the maximum efficiency is bounded near 50%.

Nomenclature

$\mathbf{E}, \mathbf{B}$	Electric and Magnetic Field
$\mathbf{J}$	Current Density Vector
$\mathbf{A}$	Magnetic Vector Potential
T	Thrust
$\dot{m}$	Mass Flow Rate
P	Power
σ	Complex Frequency Dependent Plasma Conductivity
e	Elementary Charge
n_e	Plasma Electron Density
m_e	Mass of Electron
ω	Applied Excitation Frequency
ω_{pe}	Plasma Frequency
c	Speed of Light
μ_0, ϵ_0, Z_0	Permeability, Permittivity, and Impedance of Free Space
r_0	Antenna Length Scale
l	Antenna Plasma Separation Distance
ν_e	Electron Collision Frequency
δ, k	Skin Depth and inverse Skin Depth
I	Current
γ, α	Non-dimensional Coupling Parameters
θ	Phase
R	Resistance
η	Thruster Efficiency

*Graduate Student, Mechanical and Aerospace Engineering Department, Research Assistant.
†Chief Scientist, EPPDyL; Professor, Applied Physics Group; AIAA Fellow

I. Introduction

The Direct Wave-Drive Thruster (DWDT) is a propulsion concept that utilizes electrostatic waves for direct momentum transfer to a plasma. Many previous waves-based thruster concepts have used various waves to heat a plasma and obtain thrust via expansion through a magnetic nozzle.[1–3] In contrast, a DWDT avoids some of the efficiency limitations associated with a magnetic nozzle[4,5] by coupling wave momentum directly into a plasma for acceleration.

While both electromagnetic and electrostatic waves can be used to heat a plasma,[1–3,6,7] electromagnetic waves are not suited for a DWDT because they contain very little momentum. However, unlike their electromagnetic counterparts, electrostatic waves have substantial momentum, and importantly, that momentum is carried primarily by the plasma particles themselves rather than the electromagnetic fields.[8] A DWDT, such as the recently proposed ponderomotive (PM) concept with beating electrostatic waves,[9] can couple the embedded momentum from an electrostatic wave directly into the plasma to achieve thrust without a nozzle.

While electrostatic waves can be excited with an antenna immersed in a plasma,[10] this would eliminate a key benefit of a waves-based thruster - that it operates without exposing surfaces to potentially life-limiting erosion processes. Therefore, an attractive option is to couple to the plasma inductively, as done in experiments by Jorns and Choueiri.[11,12] Such an inductive antenna is qualitatively similar to the inductive antennas used in Pulsed Inductive Thrusters (PIT).[13,14] However, instead of discharging a single large pulse, the wave-launching antenna operates continuously.

The ponderomotive DWDT concept[9] described above has already been explored from the perspective of wave damping and plasma acceleration due to the electrostatic PM potential. However, this analysis lacks the thrust and efficiency-limiting behavior associated with the antenna-plasma interaction. Similar to a PIT, all of the momentum contained in the excited waves - and subsequently the bulk plasma - must be obtained from this inductive coupling. By analyzing this coupling, and ignoring the subsequent wave dynamics, we can derive upper bounds on the scaling of thrust and thrust efficiency for a DWDT in order to evaluate its potential as a propulsion concept.

The layout for this paper will proceed as follows. In Section II, we describe the thrust and loss mechanisms and define the key assumptions in our model. In Section III, we set up a general solution in terms of the magnetic vector potential generated by the antenna and solve for the force and dissipation in an annular geometry. In Section IV, we complete a parameter space investigation of the scaling of both the thrust and thrust efficiency. In Section V, we summarize the implications for the design criteria of DWDTs.

II. DWDT Modeling Assumptions

The goal of this paper is to investigate the thrust and thrust efficiency scaling of a DWDT. This can be accomplished by analyzing the momentum imparted to a plasma by an inductive antenna and the loss mechanisms associated with this momentum transfer. For an inductive antenna, the net rate of momentum transfer is the sum of all $\mathbf{J} \times \mathbf{B}$ forces in the plasma;

$$\mathbf{F} = \int \mathtt{Re}[\mathbf{J}] \times \mathtt{Re}[\mathbf{B}] dV. \tag{1}$$

We calculate the thrust efficiency scaling by determining the power losses incurred from the inductive momentum transfer. Radiative electromagnetic losses are negligible at the frequencies of interest, so the primary losses are resistive heating in the antenna and plasma. The former scales with the antenna resistance and the square of antenna current, and the plasma losses are calculated from the dissipation integral;

$$P_{\text{loss,plasma}} = \int (\mathtt{Re}[\mathbf{J}] \cdot \mathtt{Re}[\mathbf{E}]) dV. \tag{2}$$

The explicit equations for thrust and efficiency are functions of the antenna current's amplitude and frequency, the geometry of the system, and the plasma response. In this paper, we will bound the thruster performance with the simplifying assumptions. We assume the antenna has a fixed geometry based on a single length scale. We treat the plasma as a semi-infinite slab occupying a half-space at a fixed distance from the antenna. While the infinite extent is unphysical, the effects far from the antenna are negligible for the high plasma conductivities needed for efficient performance. The currents and fields in the plasma are

determined by the frequency-dependent plasma conductivity, which is primarily a function of the plasma density and electron collision frequency. Finally, we assume the plasma slab near the antenna has a constant density in space and time, which holds only if the plasma generation source can replenish accelerated plasma sufficiency fast.

III. Magnetic Vector Potential Solution

For many geometries of interest, the magnetic vector potential will allow us to simplify the forces and losses. For example, the magnetic field of a current loop has components in both the axial and radial directions, whereas the associated **A**-field is only in the azimuthal direction. The evolution of the magnetic vector potential can be described by combining Maxwell's equations and Ohm's Law to get

$$\nabla^2 \mathbf{A} - \frac{1}{c^2}\frac{\partial^2 \mathbf{A}}{\partial t^2} - \mu_0 \sigma \frac{\partial \mathbf{A}}{\partial t} = \mu_0 \mathbf{J}_0, \tag{3}$$

where σ is the frequency dependent conductivity, which is 0 in free space, $\mathbf{J}_0$ is the excitation current density in the antenna, μ_0 is the permeability of free space, and c is the speed of light. Once we have solved for **A**, we can use the following relationships to solve for the force and dissipation:

$$\mathbf{B} = \nabla \times \mathbf{A}, \tag{4}$$

$$\mathbf{E} = -\frac{\partial \mathbf{A}}{\partial t}, \tag{5}$$

$$\mathbf{J} = -\sigma \frac{\partial \mathbf{A}}{\partial t}. \tag{6}$$

We now allow all quantities to vary sinusoidally with a given frequency, such that, $\mathbf{A} = \mathbf{A}_s\, e^{i\omega t}$, where $\mathbf{A}_s$ is the spatially-varying part of **A** and is complex-valued. Therefore, the complex, frequency dependent conductivity, σ, can be obtained from the electron momentum equation;

$$\sigma = \frac{e^2 n_e}{m(\nu_e + i\omega)} = \frac{1}{\mu_0}\frac{\omega_{pe}^2}{c^2}\frac{1}{\nu_e + i\omega}, \tag{7}$$

where m_e is the mass of an electron, n_e is the electron density, ν_e is the electron collision frequency.

Finally, we assume that the input frequencies are sufficiently small that the second-order derivative is negligible, such that

$$\nabla^2 \mathbf{A} - \frac{\omega_{pe}^2}{c^2}\frac{i\omega}{\nu_e + i\omega}\mathbf{A} = \mu_0 \mathbf{J}_0. \tag{8}$$

Once we know **A**, we can combine Eqs. 1, 2, and 4-6 to get the following equations for the net force and power dissipation:

$$\mathbf{F} = \int \mathtt{Re}[-\frac{\omega_{pe}^2}{\mu_0 c^2}\frac{i\omega}{\nu_e + i\omega}\mathbf{A}] \times \mathtt{Re}[\nabla \times \mathbf{A}]dV, \tag{9}$$

$$P_{\text{loss,plasma}} = \int (\mathtt{Re}[-\frac{\omega_{pe}^2}{\mu_0 c^2}\frac{i\omega}{\nu_e + i\omega}\mathbf{A}] \cdot \mathtt{Re}[-i\omega\mathbf{A}])dV. \tag{10}$$

A. Vector Potential Solution in an Annular Geometry

We will solve for the magnetic vector potential in an annular geometry, based on the PM concept proposed by Jorns and Choueiri.[9] The antenna is assumed to be a flat annulus with inner radius r_0 and outer radius $2r_0$ and is positioned parallel to a flat plasma surface at a stand-off distance l as shown in Figure 1. Due to the azimuthal symmetry, **A** has components only in the $\hat{\theta}$ direction.

The general method we use for solving for **A** follows closely that used by Dodd and Deeds.[15] However, we use a frequency-dependent conductivity instead of a purely real conductivity and a flat annular antenna instead of a single coil loop. This method splits the solution into three separate domains corresponding to $z < -L$, $-L < z < 0$, and $z > 0$, solves each domain separately, then matches boundary conditions in order to stitch together a unique self-consistent solution, noting that σ is zero outside the plasma. The solution domains are shown in Figure 1. To proceed, we non-dimensionalize Eq. 16 using the following scheme based on the geometry described above

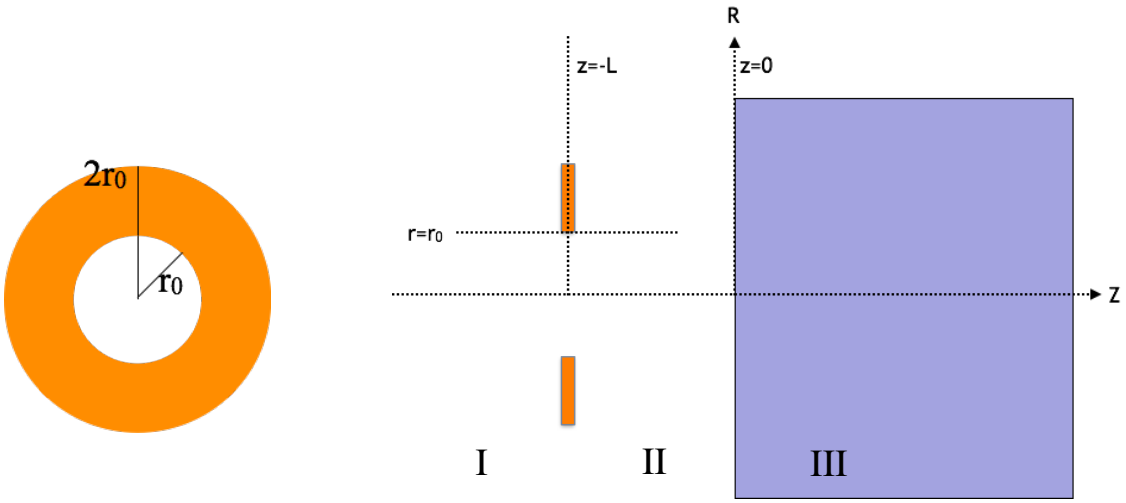

Figure 1. Antenna and Plasma Geometry. The antenna is assumed to be an annulus with inner and outer radii r_0 and $2r_0$ respectively and a total current I_a evenly distributed along the radius. The antenna is position a distance l from the surface of the plasma, which is assumed to occupy the infinite half-space $z > 0$. The geometry is therefore cylindrically symmetric about the $\hat{z}$-axis.

$$\bar{r} = \frac{r}{r_0} \qquad \bar{z} = \frac{z}{r_0} \qquad \bar{l} = \frac{l}{r_0} \qquad \delta_s = \frac{c}{\omega_{pe}} \qquad \bar{\delta}_s = \frac{\delta_s}{r_0} \qquad \bar{\nu} = \frac{\nu_e}{\omega} \qquad \tau = \omega t,$$

where $\bar{r}, \bar{z}$ are the normalized coordinates of the system, $\bar{l}$ is the normalized antenna-plasma separation distance, δ_s is the classical plasma skin depth, and $\bar{\nu}$ is the electron collision frequency normalized by the excitation frequency, ω.

In region I and II in Figure 1, there is no plasma, so the vector potential diffusion equation becomes

$$\nabla^2 \mathbf{A} = 0, \tag{11}$$

where ∇ is now the spatial gradient with respect to the normalized coordinate system. In region III, the equation becomes

$$\nabla^2 \mathbf{A}_s - \bar{\delta}_s^{-2} \frac{1}{\sqrt{1+\bar{\nu}^2}} e^{i \tan^{-1} \bar{\nu}} \mathbf{A}_s = 0. \tag{12}$$

Finally, we can define one more simplifying non-dimensional parameter, $\theta_\nu = \tan^{-1} \bar{\nu}$, where θ_ν is between 0 and $\frac{\pi}{2}$, so that

$$\nabla^2 \mathbf{A}_s - \bar{\delta}_s^{-2} \cos\theta_\nu e^{i\theta_\nu} \mathbf{A}_s = 0, \tag{13}$$

which can be expanded in our cylindrical coordinate system as

$$\frac{1}{\bar{r}} \frac{\partial}{\partial \bar{r}} (\bar{r} \frac{\partial \mathbf{A}_s}{\partial \bar{r}}) - \frac{\mathbf{A}_s}{\bar{r}^2} + \frac{\partial^2 \mathbf{A}_s}{\partial \bar{z}^2} - \bar{\delta}_s^{-2} \cos\theta_\nu e^{i\theta_\nu} \mathbf{A}_s = 0. \tag{14}$$

In order to calculate the forces and dissipation, we only need to know $\mathbf{A}$ in region III, but we need to solve the equations in all three regions simultaneously. The full derivation is performed in Appendix A for a single plasma layer and a full annular antenna with our complex conductivity and normalization inserted such that

$$\mathbf{A_3}_s = \mu_0 I_a \int_0^\infty \int_1^2 x J_1(ax) J_1(a\bar{r}) \frac{a}{a + \sqrt{a^2 + \bar{\delta}_s^{-2} \cos\theta_\nu e^{i\theta_\nu}}} e^{-a\bar{l}} e^{-\sqrt{a^2 + \bar{\delta}_s^{-2} \cos\theta_\nu e^{i\theta_\nu}}\, \bar{z}} dx da, \tag{15}$$

where I_a is the amplitude of the total azimuthal current in the antenna, J_1 is a Bessel function of the first kind, a represents the integration over the spatial separation constant, and x represents the integration over the full surface of the generating antenna in normalized coordinates. The time-dependent solution is further

normalized by defining $\bar{\mathbf{A}} = \frac{\mathbf{A}}{\mu_0 I_a}$, such that

$$\bar{\mathbf{A}}(\bar{r},\bar{z},\bar{k}_s,\bar{l},\theta_\nu,\tau) = e^{i\tau}\int_0^\infty\int_1^2 xJ_1(ax)J_1(a\bar{r})\frac{a}{a+\sqrt{a^2+\bar{\delta}_s^{-2}\cos\theta_\nu e^{i\theta_\nu}}}e^{-a\bar{l}}e^{-\sqrt{a^2+\bar{\delta}_s^{-2}\cos\theta_\nu e^{i\theta_\nu}}\,\bar{z}}dxda. \quad (16)$$

B. Force and Power Dissipation

The net force generated is given by Eq. 9, and can be re-expressed through the normalization scheme given in the previous section

$$\mathbf{F} = \mu_0 I_a^2 \int \mathtt{Re}[-\bar{\delta}_s^{-2}\cos\theta_\nu e^{i\theta_\nu}\bar{\mathbf{A}}]\times\mathtt{Re}[\nabla\times\bar{\mathbf{A}}]d\bar{V}. \quad (17)$$

Since $\mathbf{A}$ is only in the $\hat{\theta}$ direction, we can rewrite the force into components as

$$F_r = -\mu_0 I_a^2\bar{\delta}_s^{-2}\cos\theta_\nu\int \mathtt{Re}[e^{i\theta_\nu}\bar{\mathbf{A}}]\cdot\mathtt{Re}[\frac{1}{\bar{r}}\frac{\partial}{\partial\bar{r}}(\bar{r}\bar{\mathbf{A}})]d\bar{V}, \quad (18)$$

$$F_z = -\mu_0 I_a^2\bar{\delta}_s^{-2}\cos\theta_\nu\int \mathtt{Re}[e^{i\theta_\nu}\bar{\mathbf{A}}]\cdot\mathtt{Re}[\frac{\partial\bar{\mathbf{A}}}{\partial\bar{z}}]d\bar{V}, \quad (19)$$

where we are primarily concerned with the thrust direction, $\hat{z}$. Time-averaging the total axial force gives us the net thrust;

$$T = \langle F_z\rangle = \frac{1}{2\pi}\int_0^{2\pi} d\tau\cdot -\mu_0 I_a^2\bar{\delta}_s^{-2}\cos\theta_\nu\int \mathtt{Re}[e^{i\theta_\nu}\bar{\mathbf{A}}]\cdot\mathtt{Re}[\frac{\partial\bar{\mathbf{A}}}{\partial\bar{z}}]d\bar{V}. \quad (20)$$

Similarly, we compute the time-averaged power dissipation in Eq. 10 to get

$$\langle P_{\text{loss,plasma}}\rangle = \frac{1}{2\pi}\int_0^{2\pi} d\tau\cdot Z_0 I_a^2\bar{\delta}_s^{-3}\frac{\omega}{\omega_{pe}}\cos\theta_\nu\int_0^\infty\int_0^\infty\left\{\mathtt{Re}[e^{i\theta_\nu}\bar{\mathbf{A}}]\cdot\mathtt{Re}[i\bar{\mathbf{A}}]\right\}\bar{r}d\bar{r}d\bar{z}, \quad (21)$$

where Z_0 is the impedance of free space given by $\sqrt{\frac{\mu_0}{\epsilon_0}}$.

Careful treatment of the real and imaginary components of $\mathbf{A}$ and the exponential terms allow us to recast Eqs. 20 and 21 into the following forms, which are dependent only on the complex-amplitude of $\mathbf{A}$:

$$\langle F_z\rangle = \frac{\pi}{2}\mu_0 I_a^2\bar{\delta}_s^{-2}\cos^2\theta_\nu\int_0^\infty\|\bar{\mathbf{A}}_s(\bar{r},\bar{z}=0,\bar{\delta}_s,\bar{l},\theta_\nu)\|^2\bar{r}d\bar{r} \quad (22)$$

$$\langle P_{\text{loss,plasma}}\rangle = \pi Z_0 I_a^2\bar{\delta}_s^{-3}\frac{\nu_e}{\omega_{pe}}\cos^2\theta_\nu\int_0^\infty\int_0^\infty\|\bar{\mathbf{A}}_s(\bar{r},\bar{z},\bar{\delta},\bar{l},\theta_\nu)\|^2\bar{r}d\bar{r}d\bar{z}. \quad (23)$$

The maximum force occurs as $\bar{\delta}_s,\bar{l},\theta_\nu\to 0$, i.e., when the plasma density is sufficiently high and the electron collision frequency sufficiently small that the plasma perfectly shields out all magnetic fields and the stand-off distance is negligibly small. We calculate this maximum force in Appendix B;

$$\langle F_z\rangle_{max} = \frac{3}{4}\pi\mu_0 I_a^2. \quad (24)$$

This result in unsurprising, as the maximum force is equal to the magnetic pressure between two infinite current sheets[16] multiplied by the area of the antenna and an additional factor of $\frac{1}{2}$ to account for the average over the period of oscillation. We normalize by this maximum force such that

$$\langle F_z\rangle(\bar{\delta}_s,\bar{l},\theta_\nu,I_a) = \langle F_z\rangle_{max}\cdot\gamma(\bar{\delta}_s,\bar{l},\theta_\nu), \quad (25)$$

where

$$\gamma(\bar{\delta}_s,\bar{l},\theta_\nu) = \int_0^\infty\frac{2}{3}\bar{r}\left\|\int_0^\infty\int_1^2 xJ_1(ax)J_1(a\bar{r})\frac{a\bar{\delta}_s^{-1}\cos\theta_\nu}{a+\sqrt{a^2+\bar{\delta}_s^{-2}\cos\theta_\nu e^{i\theta_\nu}}}e^{-a\bar{l}}dxda\right\|^2 d\bar{r} \quad (26)$$

and is between 0 and 1.

A similar normalization can be computed for the losses associated with Joule-heating in the plasma. We separate the loss term into a portion dependent only on the antenna current and the ratio of ν_e to ω_{pe} and a non-dimensional part dependent on the other parameters of the system.

$$\langle P_{\text{loss,plasma}}\rangle(\bar{\delta}_s, \bar{l}, \theta_\nu, I_a, \omega) = \frac{3}{4}\pi Z_0 I_a^2 \frac{\nu_e}{\omega_{pe}} \cdot \alpha(\bar{\delta}_s, \bar{l}, \theta_\nu), \tag{27}$$

where

$$\alpha(\bar{\delta}_s, \bar{l}, \theta_\nu) = \bar{\delta}_s^{-1} \int_0^\infty \int_0^\infty \frac{4}{3}\bar{r} \left\| \int_0^\infty \int_1^2 x J_1(ax) J_1(a\bar{r}) \frac{a\bar{\delta}_s^{-1}\cos\theta_\nu}{a + \sqrt{a^2 + \bar{\delta}_s^{-2}\cos\theta_\nu e^{i\theta_\nu}}} e^{-a\bar{l}} e^{-\sqrt{a^2+\bar{\delta}_s^{-2}\cos\theta_\nu e^{i\theta_\nu}}\,\bar{z}} dx da \right\|^2 d\bar{r} d\bar{z}, \tag{28}$$

and is also between 0 and 1.

IV. Parameter Space Investigation

A. Thrust and Power Dissipation

At this point, we have analytical descriptions for the thrust and power dissipation as functions of the total current in the antenna, I_a, the electron collision frequency, ν_e, and three non-dimensional parameters, $\bar{\delta}_s$, $\bar{l}$, and θ_ν. The interplay of these three parameters is seen in the large integral equations for γ and α. These equations do not have explicit solutions in terms of elementary functions and therefore we performed numerical integrations over a parameter space from $\bar{\delta}_s = 1$ to $\frac{1}{64}$, $\bar{l} = 1$ to $\frac{1}{16}$, and $\bar{\nu} = 0$ to 10 ($\theta_\nu = 0$ to 1.47).

Figure 2 shows contour plots for the coupling parameter, γ, in terms of $\bar{\delta}_s$ and $\bar{l}$ for various values of $\bar{\nu}$. As expected, we can see that γ increases towards unity as $\bar{\delta}_s, \bar{l}, \bar{\nu} \to 0$. As the reverse happens, γ quickly decreases to zero as $\bar{\delta}_s, \bar{l}, \bar{\nu}$ approach order 1. γ does not exhibit large changes for $\bar{\nu} < 1$, which corresponds to $\omega \gg \nu_e$.

Figure 3 shows similar contour plots for dissipation parameter, α, in terms of the same parameter space. α and γ exhibit similar behavior, such that as γ increases, the dissipation losses also increase. Qualitatively, this occurs because more current must be present in the plasma in order to increase the net force. This additional current leads to more ohmic losses.

B. Efficiency

Given the assumption of constant density and infinite plasma extent described in Section II, the calculated thrust efficiency, defined by

$$\eta = \frac{P_{\text{thrust}}}{P_{\text{thrust}} + \langle P_{\text{loss,plasma}}\rangle + \langle P_{\text{loss,antenna}}\rangle}, \tag{29}$$

is expected to be an upper bound. Using Eq. 22, the thrust power is

$$P_{\text{thrust}} = \frac{T^2}{2\dot{m}} = \frac{9\pi^2\mu_0^2 I_a^4 \gamma^2}{32\dot{m}}, \tag{30}$$

and the time-averaged resistive loss in an antenna with effective resistance R_{eff} is

$$\langle P_{\text{loss,antenna}}\rangle = \frac{1}{2} R_{\text{eff}} I_a^2. \tag{31}$$

Combining Eqs. 27 and 29-31, we can express thrust efficiency in terms of the normalized dissipation integrals associated with the antenna and plasma.

$$\eta = \frac{1}{1 + P_{D,\text{plasma}} + P_{D,\text{antenna}}}. \tag{32}$$

$$P_{D,\text{plasma}} = \frac{8\dot{m}Z_0}{3\pi\mu_0^2 I_a^2} \frac{\nu_e}{\omega_{pe}} \frac{\alpha}{\gamma^2}. \tag{33}$$

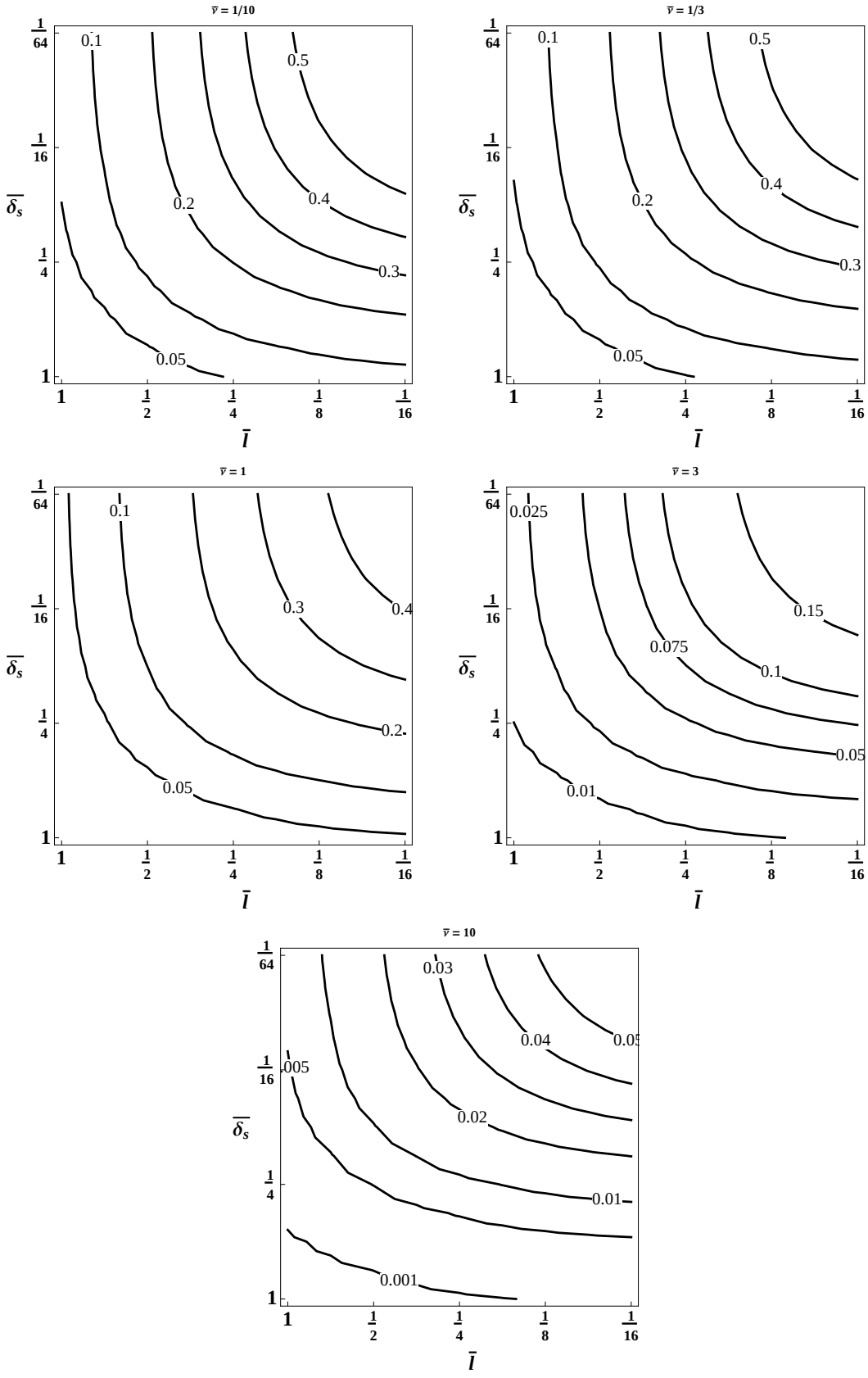

Figure 2. Contour Plots of the coupling parameter γ as a function of the normalized skin-depth, the normalized stand-off distance, and the normalized electron collision frequency. Contours of γ are plotted on Log-Log plots of the antenna-plasma coupling length and the inverse of the plasma skin depth. The five plots correspond to varying electron collision frequencies.

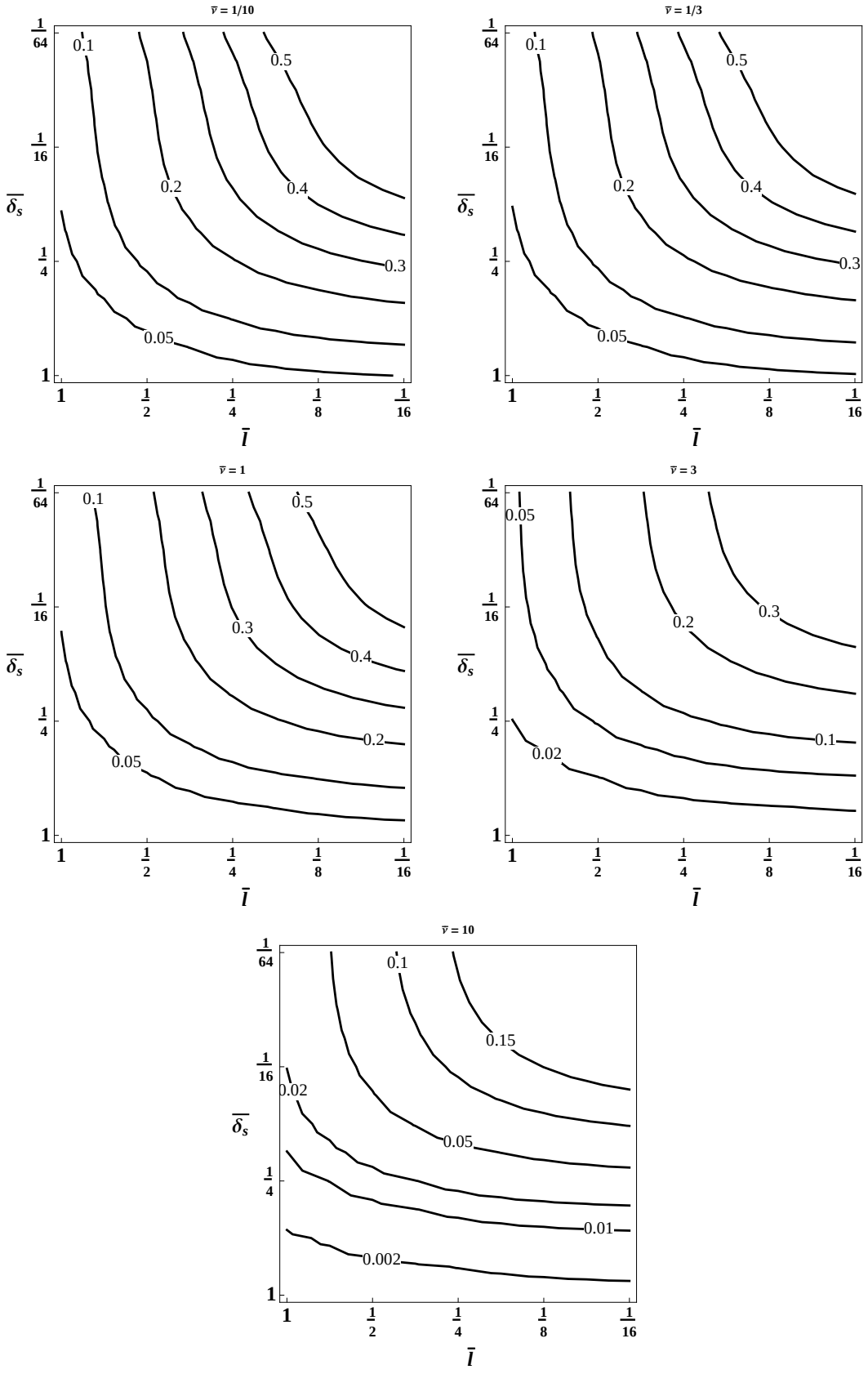

Figure 3. Contour Plots of the dissipation parameter α as a function of the normalized skin-depth, the normalized stand-off distance, and the normalized electron collision frequency. Contours of α are plotted on Log-Log plots of the antenna-plasma coupling length and the inverse of the plasma skin depth. The five plots correspond to varying electron collision frequencies.

$$P_{D,\text{antenna}} = \frac{16\dot{m}R_{\text{eff}}}{9\pi^2\mu_0^2 I_a^2\gamma^2}. \tag{34}$$

Efficiency is improved by minimizing the normalized dissipation integrals. This improvement can be achieved by increasing the total current in the antenna - and therefore the total power of the device. At a fixed current level, the antenna dissipation is minimized by increasing the coupling parameter γ. However, since α scales with γ, the plasma dissipation requires minimizing the ratio $\frac{\alpha}{\gamma^2}$. Contour plots in Figure 6 show that $\frac{\alpha}{\gamma^2}$ decreases as the skin depth, stand-off length, and electron collision frequency decrease.

Figure 5 shows plots of efficiency as a function of power for a range of scaling parameters by assuming that $R_{\text{eff}} = 0$ and choosing a typical mass flow rate of 1 mg/s. At a fixed input power, efficiency increases for smaller stand-off distances and electron collision frequencies, but efficiency decreases for smaller skin-depths. This result can occur because increasing the coupling increases the power requirements for a given I_a. However, as shown in Figure 7, this trend reverses for sufficiently large antenna resistances, in which case, improved coupling always results in higher efficiencies.

V. Conclusion

The Direct Wave-Drive Thruster is an electrode-less and nozzle-less propulsion concept, which confers potential advantages compared to other electric devices. We have analytically modeled the thrust and thrust efficiency of the DWDT concept, and shown the scaling depends on two coupling parameters, γ and α, which themselves are functions of three important non-dimensional parameters: $\bar{\nu}$, $\bar{l}$, and $\bar{\delta}_s$. In general, efficiency increases as $\bar{\nu}$, $\bar{l}$, and $\bar{\delta}_s$ become small.

Practically, since the ν_e is not easily controlled, the requirement $\bar{\nu} < 1$ suggests an optimal frequency range for wave excitation such that $\omega > \nu_e$, but not so large as to reach the electromagnetic regime. The stand-off distance, l, includes the physical antenna width and any necessary insulation. Therefore, the size of a DWDT, r_0, must be sufficiently large compared to these thicknesses. Finally, the antenna must also be large compared to the skin depth of the plasma. While we can attempt to minimize skin depth by increasing the plasma density, this results in larger collision frequencies as well, which may be counterproductive.

To put the above model in perspective by making reasonable physical assumptions; for $\dot{m} = 1\,\text{mg/s}$, $R_{\text{eff}} = 1\,\text{m}\Omega$, $r_0 = 5\,\text{cm}$, $l = 1\,\text{cm}$, $n_e = 10^{18}\,\text{m}^{-3}$, and $T_e = 3\,\text{eV}$, a 5 kW thruster would have efficiency bounded near 50%.

Two key assumptions were made about the plasma in this model that are expected to over-estimate the performance: the plasma is infinite in extent and has a constant density in space and time near the antenna. For sufficiently large coupling, the plasma currents occur near the antenna, and so the force and dissipation are not substantially changed by assuming a large plasma extent. The constant density assumption, however, ignores the wave-damping and absorption dynamics. Including these processes could have substantial effects on the scaling of the DWDT, and must be taken into account in order to determine more precise scaling.

Appendix A

Starting with Eqs. 19 and 22, we apply separation of variables of $\mathbf{A}_s$ such that

$$\mathbf{A}_S = R(\bar{r}) \cdot Z(\bar{z}), \tag{35}$$

and define a separation constant a^2. Therefore, the solution can be described by

$$\frac{1}{\bar{r}R}\frac{\partial}{\partial\bar{r}}(\bar{r}\frac{\partial R}{\partial\bar{r}}) - \frac{1}{\bar{r}^2} = -a^2 \tag{36}$$

$$\frac{1}{Z}\frac{\partial^2 Z}{\partial\bar{z}^2} = a^2 + b^2, \tag{37}$$

where $b^2 = \bar{\delta}_s^{-2}\cos\theta_\nu e^{i\theta_\nu}$ in region III, and $b = 0$ in regions I and II, outside the plasma. The solutions to the R equation are Bessel functions of the 1st and 2nd kind. However, only Bessel functions of the first kind are physical. The Z equation has growing and decaying exponential solutions, where physically region I can only have growing exponentials and region III can only have decaying exponentials.

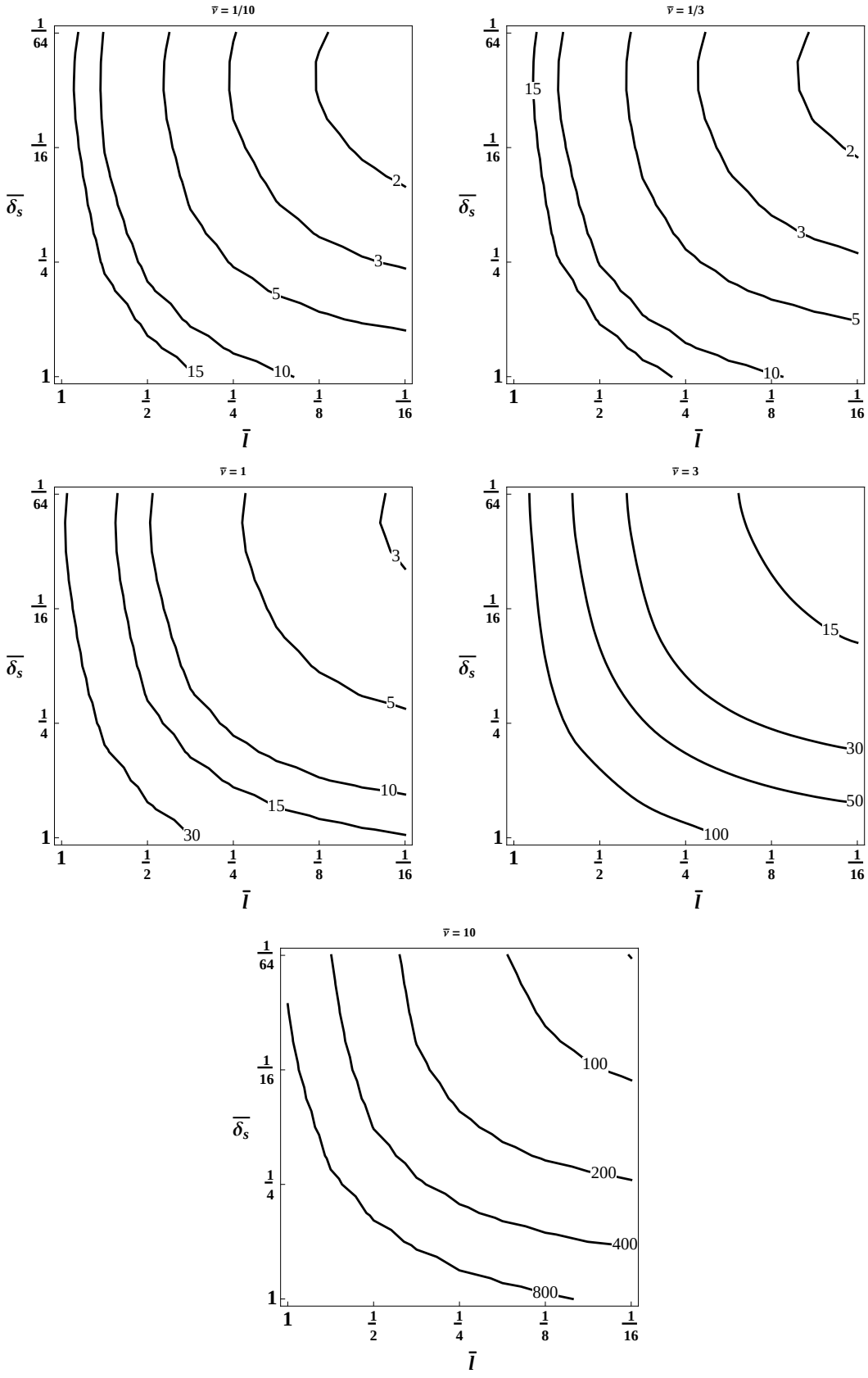

Figure 4. Contour Plots of $\frac{\alpha}{\gamma^2}$ as a function of the normalized skin-depth, the normalized stand-off distance, and the normalized electron collision frequency. Contours of $\frac{\alpha}{\gamma^2}$ are plotted on Log-Log plots of the stand-off distance and the inverse of the plasma skin depth. The five plots correspond to varying electron collision frequencies.

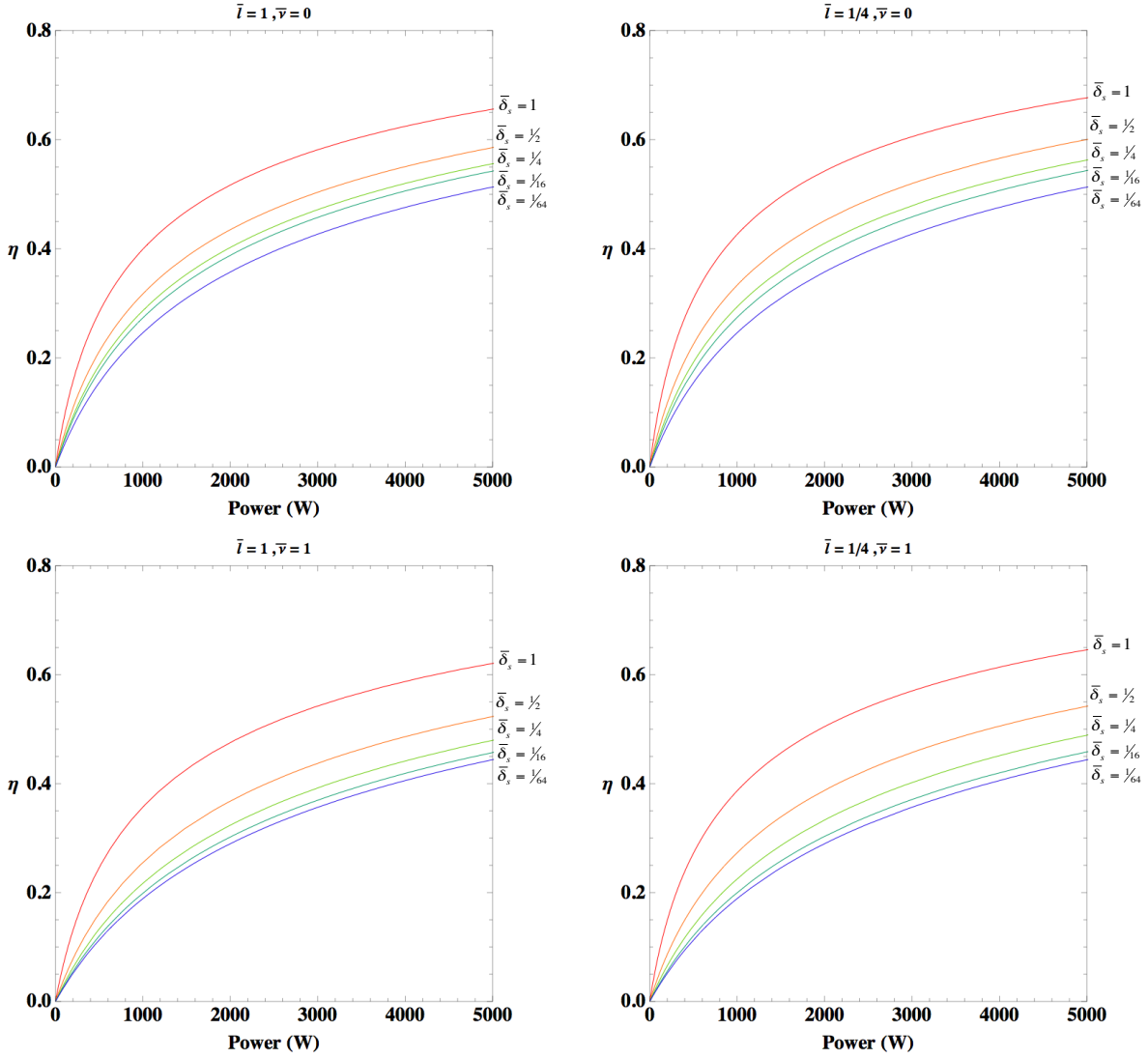

Figure 5. Efficiency vs. Power. Assuming $\dot{m} = 1\,\mathrm{mg/s}$, $\nu_e/\omega_{pe} = 10^{-4}$, $R_{\mathbf{eff}} = 0$. The left-side plots are for $\bar{l} = 1$ and the right-side are for $\bar{l} = 1/4$. The upper plots have $\bar{\nu} = 0$ and the lower plots have $\bar{\nu} = 1$, which corresponds to $\nu_e = 0$ and $\nu_e = \omega$ respectively. Efficiency is plotted against total input power for various $\bar{\delta}_s$. $\bar{\delta}_s = 1$ gives the best efficiency in red and $\bar{\delta}_s = 1/64$ gives the worst efficiency in purple.

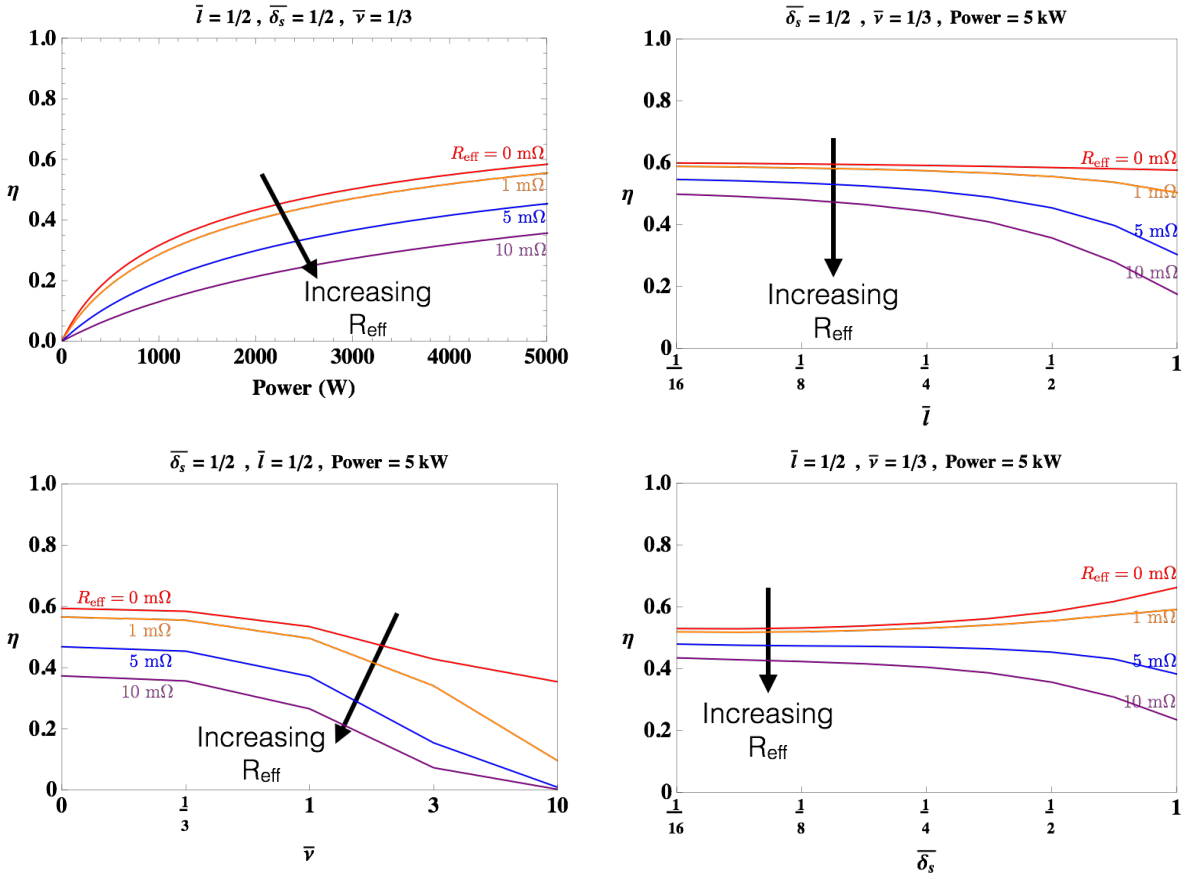

Figure 6. Efficiency vs Power, Normalized Stand-off Distance, Normalized Electron Collision Frequency, and Normalized Plasma Skin Depth.

As a result, the solutions to Eqs 19 and 22 in each region are:

$$\mathbf{A_1}_s(\bar{r},\bar{z}) = \int_0^\infty \left[C_1(a)e^{a\bar{z}}J_1(a\bar{r})\right]da \tag{38}$$

$$\mathbf{A_2}_s(\bar{r},\bar{z}) = \int_0^\infty \left[\left(C_2(a)e^{a\bar{z}} + C_3(a)e^{-a\bar{z}}\right)J_1(a\bar{r})\right]da \tag{39}$$

$$\mathbf{A_3}_s(\bar{r},\bar{z}) = \int_0^\infty \left[C_4(a)e^{-b\bar{z}}J_1(a\bar{r})\right]da. \tag{40}$$

Dodd and Deeds previously generated and solved similar equations assuming a single coil loop and multiple conducting layers of material. We proceed using their methodology, but instead of a single loop, we have a full annular antenna, so we will use their solution and integrate over many loops to form a full flat annulus. Assuming the single coil loop has a radius x in normalized coordinates, the appropriate boundary conditions are:

$$\mathbf{A_1}_s(\bar{r},-\bar{l}) = \mathbf{A_2}_s(\bar{r},-\bar{l}) \tag{41}$$

$$\mathbf{A_2}_s(\bar{r},0) = \mathbf{A_3}_s(\bar{r},0) \tag{42}$$

$$\frac{\partial \mathbf{A_1}_s}{\partial \bar{z}}|_{\bar{z}=-\bar{l}} = \frac{\partial \mathbf{A_2}_s}{\partial \bar{z}}|_{\bar{z}=-\bar{l}} + \mu_0 I\delta(\bar{r}-x) \tag{43}$$

$$\frac{\partial \mathbf{A_2}_s}{\partial \bar{z}}|_{\bar{z}=0} = \frac{\partial \mathbf{A_3}_s}{\partial \bar{z}}|_{\bar{z}=0}. \tag{44}$$

which forms four equations for four knowns. Therefore, we have

$$C_1(a) = \frac{1}{2}\mu_0 I x J_1(ax)\left[\frac{a-b}{a+b}e^{-a\bar{l}} + e^{a\bar{l}}\right] \tag{45}$$

$$C_2(a) = \frac{1}{2}\mu_0 I x J_1(ax)\frac{a-b}{a+b}e^{-a\bar{l}} \tag{46}$$

$$C_3(a) = \frac{1}{2}\mu_0 I x J_1(ax)e^{-a\bar{l}} \tag{47}$$

$$C_4(a) = \mu_0 I x J_1(ax)\frac{a}{a+b}e^{-a\bar{l}}. \tag{48}$$

In order to calculate the forces and losses in the plasma, we are solely concerned with region III, and the magnetic vector potential in that region is:

$$\mathbf{A_3}_{\text{loop}}(\bar{r},\bar{z}) = \mu_0 I \int_0^\infty \left[xJ_1(ax)J_1(a\bar{r})\frac{a}{a+b}e^{-a\bar{l}}e^{-b\bar{z}}\right]da. \tag{49}$$

A full annulus with inner radius r_0 and outer radius $2r_0$ can be thought of as many individual coils with radii between r_0 and $2r_0$, which correspond to $x = 1$ and $x = 2$ in the normalized coordinate system. Each individual coil has a fraction of the total antenna current, I_a. Taking the limit of behavior as infinitely many coils with I_a evenly distributed amongst them, we get a total magnetic vector potential by integrating over x:

$$\mathbf{A_3}_s(\bar{r},\bar{z}) = \mu_0 I_a \int_1^2 \int_0^\infty \left[xJ_1(ax)J_1(a\bar{r})\frac{a}{a+b}e^{-a\bar{l}}e^{-b\bar{z}}\right]dadx. \tag{50}$$

Appendix B

Limiting Case of the Time Averaged Force

In this section, we will show that the maximum time averaged force in the limiting case where $\bar{\delta}_s, \bar{l}, \theta_\nu \to 0$ is correctly given in Eq. 34. This can be demonstrated by showing that $\gamma \to 1$. Recall from Eq. 26

$$\gamma(\bar{\delta}_s, \bar{l}, \theta_\nu) = \int_0^\infty \frac{2}{3}\bar{r} \left\| \int_0^\infty \int_1^2 x J_1(ax) J_1(a\bar{r}) \frac{a\bar{\delta}_s^{-1} \cos\theta_\nu}{a + \sqrt{a^2 + \bar{\delta}_s^{-2} \cos\theta_\nu e^{i\theta_\nu}}} e^{-a\bar{l}} dx da. \right\|^2 d\bar{r} \tag{51}$$

As θ_ν becomes small, $\cos\theta_\nu$ and $e^{i\theta_\nu}$ both tend towards unity. Similarly, as $\bar{l}$ decreases, $e^{-a\bar{l}} \to 1$. Finally, the large fraction in the integrand tends towards a as $\bar{\delta}_s \to 0$. Therefore,

$$\gamma(\bar{\delta}_s \to 0, \bar{l} \to 0, \theta_\nu \to 0) \to \int_0^\infty \frac{2}{3}\bar{r} \left\| \int_0^\infty \int_1^2 x J_1(ax) J_1(a\bar{r}) a dx da. \right\|^2 d\bar{r}. \tag{52}$$

The double integral in the $\|$ brackets becomes unity if $\bar{r}$ is between the limits of integration on x. Otherwise, the integrand goes to 0. Therefore,

$$\gamma(\bar{\delta}_s \to 0, \bar{l} \to 0, \theta_\nu \to 0) \to \int_1^2 \frac{2}{3}\bar{r} d\bar{r} = 1. \tag{53}$$

Acknowledgements

This research was carried out with support from the Plasma Science and Technology Program from the Princeton Plasma Physics Laboratory.

References

[1]Stallard, B.W., Hooper, E.B., Power, J.L., "Whistler-driven, electron-cyclotron-resonance-heated thruster - Experimental status," *Journal of Propulsion and Power*, Volume 12, No. 4, 1996.

[2]Diaz, F.R.C., "The Vasimr Rocket," *Scientific American*, Volume 283, pp90-97, November 2000.

[3]Pavarin, D., Ferri, F., et. al., "Design of a 50W Helicon Plasma Thruster," 31^{st} International Electric Propulsion Conference, Number IEPC-2009-205. September 20 - 24, 2009.

[4]Little, J.M., Choueiri, E.Y., "Thrust and efficiency model for electron-driven magnetic nozzles," *Physics of Plasmas*, Volume 20, Number 103501, 2013.

[5]Little, J.M., Choueiri, E.Y., "Plasma Detachment and Momentum Transfer in Magnetic Nozzles," 47^{th} Joint Propulsion Conference, Number AIAA-2011-6001. July 31-Aug 3, 2011.

[6]Jorns, B., Choueiri, E.Y., "Efficiency of Plasma Heating with Beating Electrostatic Waves," 47^{th} Jnt. Prop. Conf. Number AIAA-2011-5894. July 31- Aug 3, 2011.

[7]Jorns, B. and Choueiri, E.Y., "Ion Heating with Beating Electrostatic Waves," *Physical Review Letters*, Vol. 106, No. 8, Feb. 2011.

[8]Dodin, I.Y., and Fisch, N.J., "Axiomatic Geometrical Optics, Abraham-Minkowski controversy and photon properties derived classically," *Phys. Rev. A*, Vol 86 Issue 5, Number 053834. November 2012.

[9]Jorns, B. and Choueiri, E.Y., "Thruster concept for transverse acceleration by the beating electrostatic waves ponderomotive force," 32^{nd} International Electric Propulsion Conference, Number IEPC-2011-214, September 11-15, 2011.

[10]Spektor, R. and Choueiri, E. Y., "Measurements of Ion Energization by a Pair of Beating Electrostatic Ion Cyclotron Waves," 29^{th} International Electric Propulsion Conference, Number IEPC-2005-289, October 31 - November 4, 2005.

[11]Jorns, B. and Choueiri, E.Y., "Experiment for Plasma Energization with Beating Electrostatic Waves," 31^{st} International Electric Propulsion Conference. IEPC-09-199. Sep 21 - 24, 2009.

[12]Jorns, B. and Choueiri, E.Y., "Experimental Characterization of Plasma Heating with Beating Electrostatic Waves," 48^{th} Jnt. Prop. Conf. Number AIAA-2012-4194. July 30 - Aug 1, 2012.

[13]Lovberg, R. H., Dailey, C. L., "PIT Mark V Design." Number AIAA 1991-3571, September 1991.

[14]Choueiri, E., Polzin, K., "Faraday Accelerator with Radio-frequency Assisted Discharge (FARAD)." Number AIAA 2004-3940, July 2004.

[15]Dodd, C.V., Deeds, W.E., "Analytical Solutions to the EddyCurrent ProbeCoil Problems," *Journal of Applied Physics*, Volume 39, 1968.

[16]Purcell, E.M., *Electricity and Magnetism*, McGraw-Hill, 1985.